meteorology

Article

Northern Hemisphere Flow Regime Transitions, Blocking, and the Onset of Spring in the Central USA during Late Winter 2019 and 2021

Madeline A. Est [1,2], Samuel Mount [1], Christopher A. Steward [1] and Anthony R. Lupo [1,3,4,*]

[1] Atmospheric Science Program, School of Natural Resources, University of Missouri, Columbia, MO 65211, USA; mae4yx@mail.missouri.edu (M.A.E.); samuelmount@mail.missouri.edu (S.M.); casvf9@mail.missouri.edu (C.A.S.)
[2] KMIZ TV, 501 Buisness Loop, Columbia, MO 65201, USA
[3] Missouri Climate Center, 320 Anheuser Busch Natural Resources Building, University of Missouri, Columbia, MO 65211, USA
[4] Department of Meteorology, Climatology and Atmospheric Environment, Kazan Federal University, 5 Tovarishcheskaya, 420097 Kazan, Russia
* Correspondence: lupoa@missouri.edu; Tel.: +1-573-884-1638

Abstract: Studies have shown that maxima in the time series of Northern Hemisphere (NH) integrated enstrophy (IE) can be associated with large-scale flow regime transitions and, often, the onset and decay of blocking events. During February and March 2019, and then February 2021, strong IE maxima were associated with changes in the NH flow regimes that brought very cold conditions to the central United States. The colder conditions in the central USA during late winter 2019 and 2021 were also associated with very strong Pacific or Atlantic Region blocking events. Using the NCEP re-analyses, three different teleconnection indexes, and surface weather data from nine different cities in the central USA, IE maxima, flow regime transitions, and surface weather regimes are identified. The mean temperature and precipitation characteristics for the cities named here during the different large-scale flow regime characteristics are compared. The results have demonstrated that relatively warm conditions occurred through the first part of February 2019 before a period of anomalously colder (as much as 12 °C below normal) and drier weather, with more snow, persisted into early March. This period was bookended by maxima in the NH IE time series, changes in the character of the main NH teleconnection indexes, and a strong simultaneous NH blocking episode. Following the cold period, the temperature regime returned to values that were closer to seasonal normal values, which were then discussed as a possible indicator of a transition from a winter to a spring regime.

Keywords: blocking; integrated enstrophy; flow regime transitions; extreme temperature; prediction

check for updates

Citation: Est, M.A.; Mount, S.; Steward, C.A.; Lupo, A.R. Northern Hemisphere Flow Regime Transitions, Blocking, and the Onset of Spring in the Central USA during Late Winter 2019 and 2021. *Meteorology* **2022**, *1*, 45–63. https://doi.org/10.3390/meteorology1010005

Academic Editor: Edoardo Bucchignani

Received: 14 January 2022
Accepted: 16 February 2022
Published: 24 February 2022

Publisher's Note: MDPI stays neutral with regard to jurisdictional claims in published maps and institutional affiliations.

Copyright: © 2022 by the authors. Licensee MDPI, Basel, Switzerland. This article is an open access article distributed under the terms and conditions of the Creative Commons Attribution (CC BY) license (https://creativecommons.org/licenses/by/4.0/).

1. Introduction

During February and March 2019, simultaneously occurring East Pacific and East Atlantic–Western Europe, blocking events were likely at least partially responsible for unusually cold weather across the central USA, especially across the state of Missouri based on previous studies [1–4]. Temperature anomalies were more than one standard deviation below the respective monthly normal during late February and early March [5,6]. This same period was accompanied by snow across northern Missouri. Then, during February 2021, a very strong cold air outbreak set many cold temperature records across the central USA as far south as southern Texas. This cold wave was noteworthy for the low temperatures [5,6] as well as their persistence and caused economic disruption for the south and central USA [7].

Cold air outbreaks over the Midwest USA are often accompanied by atmospheric blocking (e.g., [1–4]). These cold air outbreaks usually occur upstream and downstream of blocking in other parts of the world as well (e.g., [3,8–13]). Additionally, many studies have noted that blocking events can have a deep vertical structure influencing the circulation of upper troposphere and into the stratosphere altering the temperature and pressure structure as well as the concentration of trace gases (e.g., [14–17]).

The work of Klaus et al. [18] demonstrated the utility of a quantity called integrated enstrophy (IE) in predicting large-scale changes in the Northern Hemisphere (NH) flow regimes, building on earlier research which showed that IE could be used to identify these flow transitions and equating IE with entropy (e.g., [19,20]). This quantity is the area integrated square of the vorticity over the NH and it will be described in more detail in section two (see Equation (1)). They [18] showed that an operationally used ensemble model can predict IE maxima with skill to at least 7 days, in both the occurrence and strength of the maximum. Some of these IE maxima were well forecast to 10 days. This predictability is consistent with the current skill of operational models to predict basic fields such as height or pressure [21,22]. They [18] also showed that significant maxima in the IE time series correlate to NH flow regime changes. For example, the NH flow regime transition event of 14 February 2019 was a case study examined by [18] in which the associated IE maximum was identified by the model ensemble about 10 days in advance.

Newberry et al. [23] developed a criterion for identifying the spring-to-summer transition period in the Missouri River Valley region in the regional large-scale flow field. They used the 500 hPa height fields as well as surface temperature to define the onset of summer, which they also showed accompanied a change in the frequency of significant rainfall events [23]. In this study, they also confirmed that the spring-to-summer transition is accompanied by a decrease in the NH wave amplitude index [24,25] and the NH IE. Seasonal transitions are not often studied in the literature [25] and a search of journal publications from the American Meteorological Society for that term in the title of articles revealed only 13 items. Others [26] (and references therein) have studied the tendency for flow regime types to change with the boreal seasons using clustering methods and found that different flow configurations will be prevalent during the warm versus cold seasons over the Eurasian continent.

The formation and predictability of blocking has been examined by several studies over the last few decades using observational data especially at onset (e.g., [27–29]) and studies are still demonstrating difficulties that models encounter even today (e.g., [30,31]) with block predictability. However, there are several aspects regarding the dynamics of the predictability of blocking that have been examined and blocking dynamics are discussed in two recent review papers on blocking (e.g., [32,33]). Models have traditionally had difficulty with forecasting the decay of blocking events, and several have related block decay to changes in the large-scale flow (e.g., [34–39]) or the lack of synoptic-scale forcing (e.g., [31,40–42]). The work of [35] was the first to suggest blocking does not survive large-scale flow regime transitions, a view echoed by [38] and [39]. However, [43] demonstrated that blocking can survive large-scale flow regime transitions if the synoptic-scale conditions are favorable.

The goals of this study is to examine the abrupt changes in the Northern Hemisphere (NH) and local large-scale flow regime as detected using IE and the association with the occurrence of atmospheric blocking events. Then, this work will examine the connection between the large-scale events described above to the severe cold outbreaks of February and March 2019 and February 2021. Lastly, the termination of the cold outbreaks will be discussed in association with a possible transition from winter to spring conditions. Special focus will be placed also on examining the dynamics for the decay of a pair of simultaneous blocking events in March 2019. This study will also discuss the predictability of large-scale flow regime changes in an ensemble model for February and March 2019 from the work of [18]. However, unlike [18], this work will use large-scale changes to guide the study of local conditions. Section two will describe the data and methods used, while section three will examine the large-scale NH flow regime changes, the regional weather, and discuss the implications. Section four will present the major conclusions of this work.

2. Materials and Methods

2.1. Data

Here, the 500 hPa height fields (m) at 1200 UTC daily during the months of February 2019, March 2019, January 2021, and February 2021 were used to calculate observed values for enstrophy. These images are provided by the National Centers for Environmental Prediction/National Center for Atmospheric Research (NCEP/NCAR) reanalyses, which provide large-scale meteorological data on 2.5° by 2.5° latitude–longitude grids [44]. The data are archived at NCAR's research facility in Boulder, CO. The Northern Hemisphere daily 500 hPa anomaly maps for the months indicated above were also used for verification in this research.

The observed atmospheric blocking characteristics were obtained from the blocking archive housed in the University of Missouri Weather Analysis and Visualization (WAV) laboratory [45]. A definition for atmospheric blocking is that these events are persistent quasi-stationary anticyclones or ridges in the mid-latitude jet stream [33]. The blocking characteristics used here were onset and termination dates, duration (days), and block intensity (BI). The blocking climatological characteristics are available for every event from 1968 to 2021.

The teleconnection indexes, specifically the AO, the North Atlantic Oscillation (NAO), and PNA, were downloaded from the Climate Prediction Center website [46,47]. These teleconnections were chosen, since they are commonly associated with weather and climate in the study region, which is defined below. In Section 3, the daily teleconnection indexes will be used to confirm that an IE maximum and flow regime change occurred by calculating the slope of the daily time series during specific periods. In order to quantify changes in the slope, a simple linear regression line was fit to each period between IE maxima to determine the magnitude or direction of these changes.

The surface weather was obtained from the local National Weather Service office websites [6] for Columbia (COU), Saint Louis (STL), Kansas City (EAX), and Springfield (SGF), all in the state of Missouri (Figure 1). Cities in states around Missouri that were used were Des Moines, Iowa (DSM), Lincoln, Illinois (ILX), Wichita, Kansas (ICT), and Little Rock, Arkansas (LIT). The Dallas-Fort Worth, Texas (DFW) weather data were also examined in order to provide a qualitative representation of how far equatorward the cold outbreaks over the southern plains in the USA were observed. This area was harder hit by the energy supply disruptions of February 2021.

Figure 1. The study region used in this work. Each star represents the locations of weather stations used in this study.

2.2. Methods

In order to determine when the NH flow regimes transitioned, the IE quantity was calculated using the data provided by [44] and the methodology of [18]. The theoretical background for the IE quantity, the development of IE, and relationship to atmospheric flow dynamics and entropy are described in detail in [18,19].

Briefly, IE is the square of relative vorticity integrated over an area [0° to 70° N] and was calculated here using Equation (1):

$$IE = \sum_{i>0} \lambda_i \approx \int_A \zeta^2 dA \tag{1}$$

where λ_i is the ith Lyapunov exponent that is greater than zero in a dynamic system, ζ is the vorticity (the curl of the wind vector), and the vorticity squared is called enstrophy (which is the dissipation tendency of a fluid) (e.g., see [19] and references therein). In (1), vorticity is calculated at 500 hPa using the height field, the geostrophic relationship, and second order finite differencing. The values poleward of 70° N were not used because of the computational issues associated with finite differencing over longitude. In order to calculate this quantity for January and February 2021, ζ was calculated using the curl of the horizontal wind and second order finite differencing, and not the geostrophic relationship since the MAtLab software included a routine to calculate this quantity.

Klaus et al. [18], identified 34 large-scale NH flow regime transitions using IE as a diagnostic tool, and this number was consistent with other studies (e.g., [20] and references therein). In Figure 2a,b, there were seven identifiable transitions (1, 9, 14, 18, 25 February and 7, 24 March) used in their work [18]. The relative IE maxima were determined using an objective criterion, that is each maximum was one standard deviation (0.042) above the time series values before and after the maximum. This criterion was adopted here.

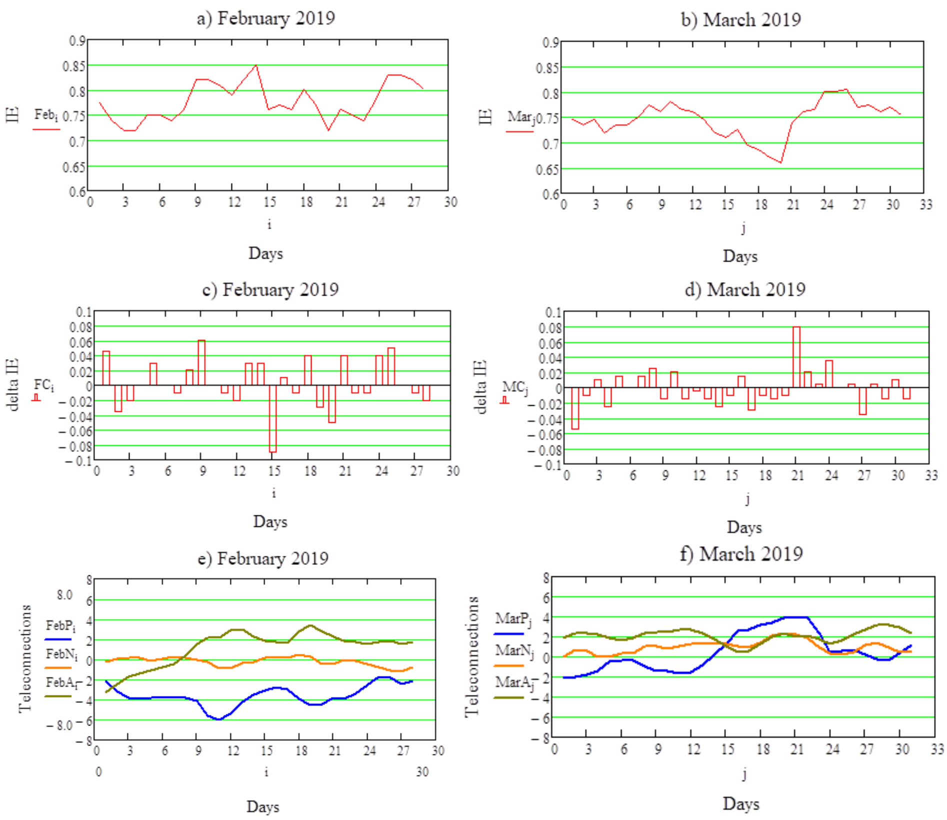

Figure 2. The Northern Hemisphere (NH) (**a**,**b**) integrated enstrophy (IE, km s^{-2}), (**c**,**d**) daily (24 h) change in IE, and (**e**,**f**) the major daily NH teleconnection indexes obtained from [47] where the AO, North Atlantic Oscillation (NAO), and PNA are grey, orange, and blue, respectively.

3. Results

3.1. Large-Scale Flows and Teleconnections

3.1.1. February and March 2019 Case

Figure 2 shows the IE, the daily change in IE, and the daily teleconnection indexes (AO, NAO, and PNA) for February (Figure 2a,c,e) and March (Figure 2b,d,f) in 2019. A comparison of Figure 2a,b would show that the mean of the February 2019 IE values were 0.031 units greater than those for March and about the same amount greater than those for January 2019 (not shown). The mean monthly IE values will be discussed further below with respect to seasonal transitions. As shown in [18] or [48], the trend or character of the daily teleconnection indexes changes qualitatively on or about the same time the IE maxima occurred.

Table 1 shows the result of the IE maxima and the teleconnection slopes and is associated with the analysis in Figures 2 and 3. In all but one case the sign changed for at least two of the three NH indexes. The exception was the 7 March 2019 case, however, there was a change in the sign for the AO index which is relevant to North American weather and the slope of the NAO (PNA) after 7 March 2019 was about 75% less (about double) than the slope before that date. Higher order polynomial fits could be undertaken for each period to better model these particular periods, however, the linear model provides strong evidence that the teleconnection indexes which represent the character of the NH flow change substantially with IE maxima.

Table 1. The slope (units day^{-1}) of a linear fit line for each daily teleconnection index in Figure 2e,f (February and March 2019) and Figure 3c (January and February 2021) during the time period between each identified IE maximum from [18].

Time Period	AO	NAO	PNA
1–9 February 2019	0.51	0.02	−0.16
9–14 February 2019	0.20	−0.03	0.23
14–18 February 2019	0.08	0.13	−0.06
18–25 February 2019	−0.24	−0.13	0.33
25 February–7 March 2019	0.02	0.16	0.19
7–24 March 2019	−0.05	0.04	0.31
24–31 March 2019	0.20	0.05	−0.00
1–17 January 2021	0.12	0.04	−0.02
17–29 January 2021	−0.14	−0.01	−0.18
29 January–10 February 2021	−0.21	−0.02	0.06
10–16 February 2021	1.09	0.10	−0.01
16–28 February 2021	0.20	0.05	−0.09

The blocking events which occurred during the 2-month period are shown in Table 2. There were eight total events, four each occurring within the Atlantic and Pacific regions as defined by Lupo et al. [49]. In the Pacific Region, 39 of the 59 days were blocked and these events occurred over the East Pacific (east of 180°). Such events have been shown to be influential on North American weather in general and over the central USA (temperature in particular) as in [3,4], and [50]. In the Atlantic, only 28 of 59 days were blocked, generally occurring over the East Atlantic. Atlantic blocking events show a weaker correlation to monthly temperatures in the central USA [4]. Six of these blocking events occurred simultaneously from about 20 February–31 March, accounting for 18 of the 40 days during this time period. This included two events in mid-March which onset within 2 days of one another and terminated on the same day. Only 16 days during these 2 months were unblocked including the first part of February and six days in Mid-March.

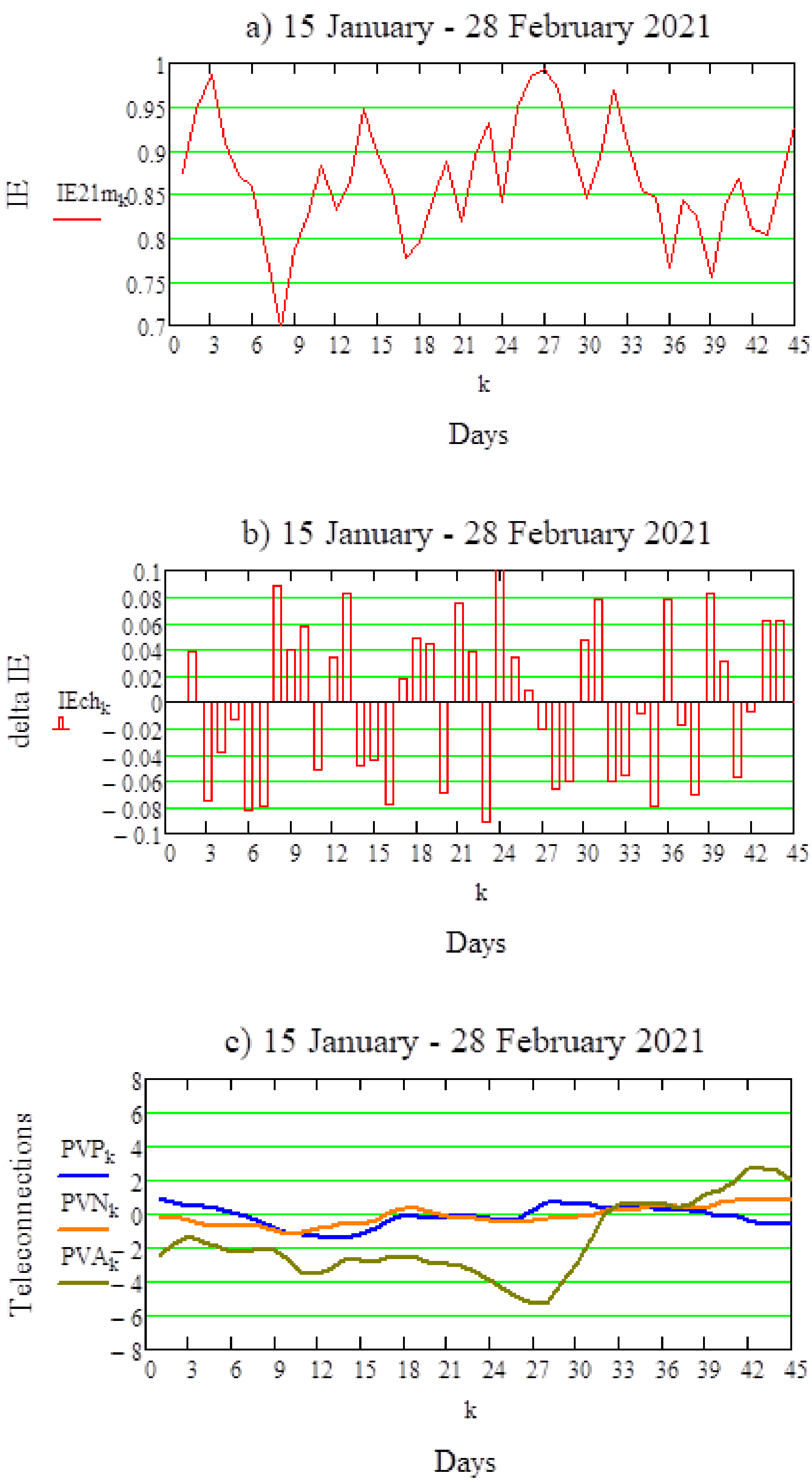

Figure 3. As in Figure 2, except for 15 January to 28 February 2021. The Northern Hemisphere (NH) (**a**) integrated enstrophy (IE, km s−2), (**b**) daily (24 h) change in IE, and (**c**) the major daily NH teleconnection indexes obtained from [47] where the AO, North Atlantic Oscillation (NAO), and PNA are grey, orange, and blue, respectively.

Table 2. The occurrence of NH blocking during the two study periods (February–March 2019 and 15 January–28 February 2021). Column one shows the regions as defined in [49], column two is the duration in days, column three shows the onset and termination time and date (UTC), column four is the block intensity (BI) and column five is the onset latitude (° N) and longitude (negative and positive are degrees W or E, respectively.

Region	Duration	Onset/Termination	BI	Onset Location
PAC	6	0000 11 February/0000 17 February 2019	3.80	40/−170
ATL	6	0000 14 February/0000 20 February 2019	3.09	45/0
ATL	9	0000 20 February/0000 1 March 2019	5.16	45/0
PAC	15	0000 23 February/0000 10 March 2019	5.02	55/−160
PAC	9	0000 16 March/0000 25 March 2019	4.50	40/−120
ATL	7	0000 18 March/0000 25 March 2019	3.33	40/−30
ATL	6.5	1200 24 March/0000 31 March 2019	3.90	50/−20
PAC	9	0000 26 March/0000 4 April 2019	4.46	55/−150
ATL	7	1200 17 January/1200 24 January 2021	4.15	52.5/−50
PAC	6	0000 22 January/0000 28 January 2021	3.32	35/−150
CON	6	0000 25 January/0000 31 January 2021	4.12	45/50
PAC	12	0000 3 February/0000 15 February 2021	4.5	35/−140
ATL	12	1200 10 February/1200 22 February 2021	4.12	60/−10
ATL	15	0000 20 February/0000 7 March 2021	3.85	40/10

3.1.2. February 2021 Case

The Polar Vortex case of February 2021 persisted for roughly 2 weeks over much of the northern and central USA and brought severe and even record-breaking cold to the south-central states causing severe disruptions to the economy. Figure 3 shows the same information as Figure 2 except for the 45-day period from 15 January–28 February 2021. Using the criterion of [18] we can identify four IE maxima (Figure 3a) during this time-period (17 and 29 January and 10 and 16 February 2021). Then, examining the behavior of the teleconnection indexes shown in Figure 3c similar to the previous case, Table 1 reveals that these four maxima were associated with a change in sign or a relatively large change in the slope for at least two of the three indexes shown here.

There were five blocking events that occurred during the 45-day period that occurred within the Atlantic and Pacific regions. In the previous case, the Pacific region experienced more blocking days, and during the 2021 period more Atlantic region blocking was observed (33 of 45 days). The Pacific region experienced only 18 blocking days, and there were 12.5 days in which blocking occurred in the NH simultaneously. Only two days were unblocked. Both Pacific Region blocking events occurred over the Eastern Pacific, while the Atlantic blocking occurred over the central and Eastern Atlantic.

3.2. Regional Weather in the Central USA

In [18], the weather conditions before and after selected flow regime changes were studied in order to differentiate the pre-transition period with the post-transition period. They used a 10-day period since the mean time-period between identified transitions was 10.7 days and the ensemble model 10-day forecasts were evaluated. Here, the choice of periods studied were governed by the occurrence of blocking events as well as the identification of IE regime transitions in Section 3.1 (Table 3). Thus, the study periods were not necessarily of equal length. In the case of February 2021, the goal was to demonstrate the profound impact of the "polar vortex" case during a winter that was otherwise warm with respect to normal. The periods used to study the surface weather characteristics here and the reason for choosing these dates is given in Table 3.

Table 3. The periods used to study the surface temperature and precipitation regimes in this section. Column 2 shows the dates and column three provides the rationale for the choice.

Period	Dates	Rationale
1	1–10 February 2019	covers the period before the 9 February IE maximum and the onset of mid-February blocking
2	11–19 February 2019	time between two IE maxima, encompasses the first period of Atlantic and Pacific region blocking
3	20 February–9 March 2019	start and end are close to IE maxima, covers a period of simultaneous blocking
4	10–15 March 2019	brief period of no blocking
5	16–24 March 2019	encompasses a second period of simultaneous blocking both terminating concurrent with an IE maximum
6	25–31 March 2019	finishes the month of March, begins another period of blocking
7	17 January–5 February 2021	time before the major cold air outbreak
8	6–19 February 2021	encompasses period of the cold air outbreak and two associated blocking events
8A	6–12 February 2021	part before onset of the Atlantic block, near the time of the 10 February IE maximum
8B	13–19 February 2021	part following onset of the Atlantic block and 16 February IE maximum
9	20–28 February 2021	time following the post cold air outbreak

The first period (1–10 February 2019) was anomalously warm across most of Missouri with only the northwest part being close to normal (Table 4) as well as the regions to the north and west (Table 5). The southern part of MO (SGF) and the southern plains (DFW and LIT) were more than one standard deviation above their respective normals (about 3.0 °C see e.g., [51]) This period was associated with a short-wave ridge at 500 hPa and 850 hPa over the middle of the USA (Figure 4A,B) and a negative PNA index (Figure 2e). An amplified long-wave ridge is also observed over the Gulf of Alaska region. Most of the region was also wetter than normal when taking the mean monthly precipitation and multiplying by the fraction of the number of days covered by the period. Not much snow was observed over the region, and northeast TX (DFW) through central KS (ICT) was dry at this time.

After the NH flow regime changed on 9 February 2019, short-lived blocking events were established in both the Pacific and Atlantic during the Period 2 (Table 3) as reflected by amplified 500 hPa ridging in the Gulf of Alaska and Western Europe (Figure 4C) for mid-February 2019. Figure 4C,D show more zonal flow across the central USA at 500 hPa and a short-wave trough at 850 hPa (Figure 4D). During this period the sign of the AO changed from negative to positive indicating more zonal flow across the NH. Accompanying this change in the flow regime over North America, all the central USA stations examined here now experienced colder than normal conditions (Tables 4 and 5). Only in northwest Missouri and into southern Iowa were the temperatures more than one standard deviation below the monthly mean. The region experienced conditions that were close to normal or wetter in terms of precipitation (Tables 4 and 5) and many areas experienced measurable snow except the western and southern stations. The cooler conditions were felt as far south as northeast Texas and central Arkansas, but the western part of the region was still relatively dry (central Kansas and northeast Texas).

The third period was markedly colder across the entire region (Tables 4 and 5) and the temperature anomalies everywhere, even as far south as Texas were more than one standard deviation below normal (except central Arkansas—LIT). Northwest Missouri (EAX) and southern Iowa (DSM) were more than two standard deviations below the normal. Across the central USA, the precipitation was close to the period normal and some of this fell as snow for seven of the nine stations (Tables 4 and 5). The 500 hPa and 850 hPa flow (Figure 4E,F) over the study region was similar to that of period 2, however there were some differences in the large-scale pattern. The PNA index trended from negative at the start of the period to near zero by the end of the period (Figure 2f). This was also the first period of long-lived simultaneous Atlantic and Pacific region blocking events, which together were the 10th strongest pair of simultaneously occurring events on record in the entire MU blocking archive (1968–2021) when simply adding the BI Index of each of the two events together. These blocking events resulted in the 500 hPa trough being located a little further equatorward than the previous period.

Table 4. The temperature anomaly (°C), precipitation (mm), and snowfall (cm) for stations in Missouri and Dallas, TX studied here, and for the periods defined in Table 3.

Period	COU	EAX	STL	SGF	DFW
1	+1.0/28.4/T	−0.2/6.3/1.3	+0.8/59.4/T	+3.1/32.7/0.3	+3.9/12.2/0
2	−2.5/18.1/8.9	−4.1/29.5/19.3	−1.8/21.6/3.6	−1.7/33.8/1.0	−1.3/17.8/0
3	−4.6/39.9/5.6	−6.7/34.8/8.6	−4.1/48.3/8.6	−3.3/34.3/2.0	−3.7/12.2/0
4	+1.5/30.7/0	+1.0/17.8/0	+1.4/27.2/0	+0.4/34.8/0	+0.3/41.4/0
5	+1.0/1.3/0	+1.3/6.4/0	−0.3/16.0/T	+0.4/6.9/0	+0.6/10.2/0
6	+0.5/52.6/T	−1.2/43.4/T	−0.2/61.7/0	+0.8/19.8/T	+0.2/2.5/0
7	+1.9/62.2/10.2	+2.8/56.9/4.6	+1.0/80.0/7.6	+1.9/69.1/5.8	+2.1/18.0/0
8	−13.3/16.2/20.6	−13.8/9.7/18.5	−12.4/20.3/22.4	−12.4/16.3/22.1	−11.4/9.7/12.7
8A	−11.3/5.6/6.1	−12.3/1.3/3.6	−9.8/5.3/3.8	−8.3/1.3/1.3	−6.0/0.3/0
8B	−15.2/10.7/14.5	−15.1/8.4/15.0	−14.5/15.0/18.5	−16.0/15.0/20.8	−16.5/9.4/12.7
9	+2.0/6.4/0.0	+2.2/0.8/0	+2.3/15.7/0	+1.0/10.7/0	+2.0/46.7/0

Table 5. As in Table 4, except for cities surrounding Missouri.

Period	DSM	ILX	LIT	ICT
1	−1.8/11.4/11.7	+0.1/30.0/4.3	+4.3/36.1/T	0.0/1.0/T
2	−6.0/24.4/38.6	−1.9/20.8/1.0	−1.0/81.0/T	−2.2/7.9/5.3
3	−8.3/40.6/18.8	−3.9/55.1/8.6	−2.4/81.5/T	−5.6/15.0/7.4
4	+0.2/30.7/T	+1.7/20.1/T	+1.5/35.8/0	+0.1/45.5/0
5	+0.3/7.1/0	−0.6/17.0/T	−1.0/11.9/0	+2.2/7.9/0
6	−0.1/7.1/0	−1.0/59.7/T	−0.6/1.5/0	+0.1/3.8/T
7	+0.3/26.9/44.5	+1.1/64.5/4.3	+2.0/32.8/0	+2.4/58.7/T
8	−13.9/8.1/17.5	−12.7/22.6/34.5	−9.4/49.3/51.6	−14.0/7.1/14.5
8A	−13.6/6.3/12.9	−10.3/8.6/11.4	−4.5/12.7/0.3	−11.6/1.5/4.3
8B	−14.2/1.8/4.6	−15.2/14.0/23.1	−14.4/36.6/51.3	−16.5/5.6/10.2
9	+1.4/6.1/5.6	+2.0/10.9/0	+0.2/78.0/0	+0.9/0.5/0

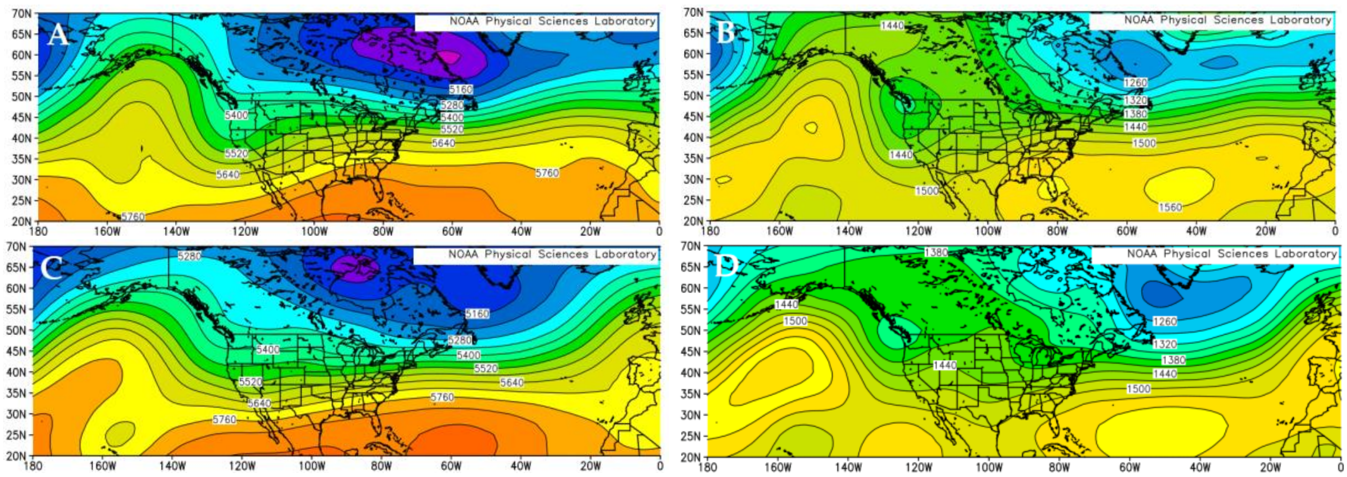

Figure 4. *Cont.*

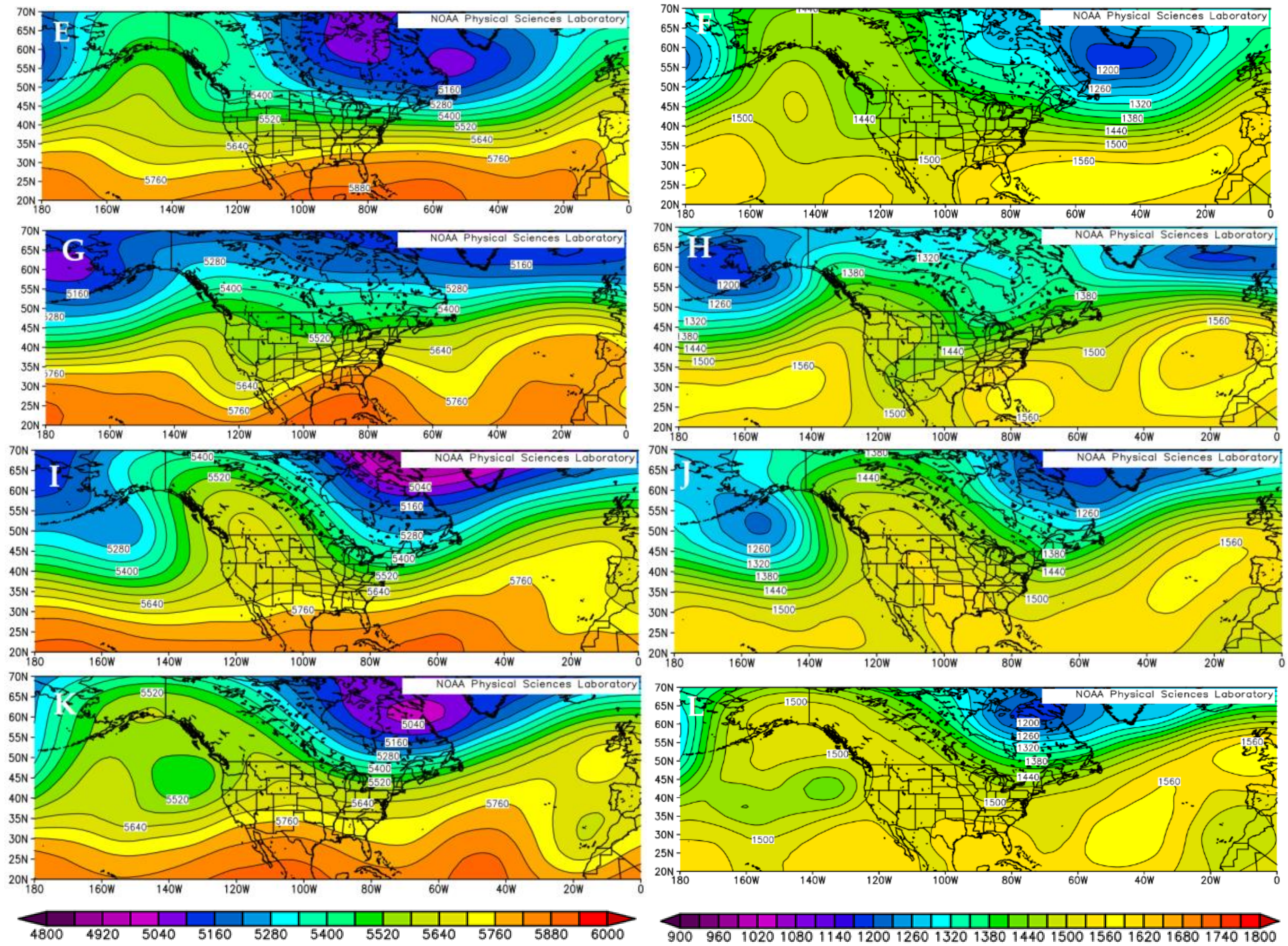

Figure 4. The 500 hPa height (m, **left**) and 850 hPa height (m, **right**) February and March 2019 periods in Table 3. The contour intervals are 60 m and 30 m, respectively. Panels (**A**,**B**), (**C**,**D**), (**E**,**F**), (**G**,**H**), (**I**,**J**), and (**K**,**L**) are for Periods 1–6, respectively.

Period 4 (10–15 March 2019) was associated with no blocking (Table 2) and the PNA Index becoming positive with a 500 hPa ridge in the west and a trough in the east (Figure 4G). At 850 hPa (Figure 4H), there was a trough over the plains states and Missouri is on the upstream part of this trough. Tables 4 and 5 demonstrate a remarkable warming over the region with most stations across the region returning to normal or above normal temperatures. The warmer air was associated with wet conditions region-wide during this short period of time. Period 5 (16–24 March 2019) was associated with another simultaneous blocking event in the Atlantic and Pacific region (Figure 4I) at 500 hPa, except this pair was not nearly as strong and the Pacific region event was located over western North America. This resulted in the temperature regime of the western part of the study region being similar to that of the previous period, but the southern and eastern part of the region returned to cooler conditions (Tables 4 and 5). The central USA was under the upstream portion of the 500 hPa and 850 hPa (Figure 4J) ridge which is typically dry.

Finally, Period 6 (25–31 March) was associated with conditions that were relatively cool compared to Period 5 for much of the region (Tables 4 and 5). The precipitation regime was normal to wet for most of Missouri and into central Illinois, but comparably dry in the southwest part of the state and elsewhere. The 500 hPa flow (Figure 4K) was similar to that of Period 5, however, the Pacific region blocking was located further west. The beginning of this period was associated with a dramatic change in the NH flow regime when the simultaneous events of Period 5 decayed abruptly. This issue will be discussed further below in Section 3.3.

For the February 2021 case, the goal is to examine the most severe part of the cold wave. Regardless of the starting and end points for this case, Period 7 and 9 were anomalously warm region-wide, while Period 8 was anomalously cold (Tables 4 and 5 and not shown). During Period 7, it was clear that the PNA Index became more negative during this time (Figure 3c), and the NAO and AO Indexes became more negative between the 17–29 January 2021 NH IE maxima (Table 1). There were two short-lived blocking events during this period, one in each ocean basin adjacent to North America, and they were of typical intensity as well [49]. During much of Period 7, the central USA including Missouri was anomalously warm and wet as the East Pacific ridge extended into the central part of North America at 500 hPa and 850 hPa (Figure 5A,B).

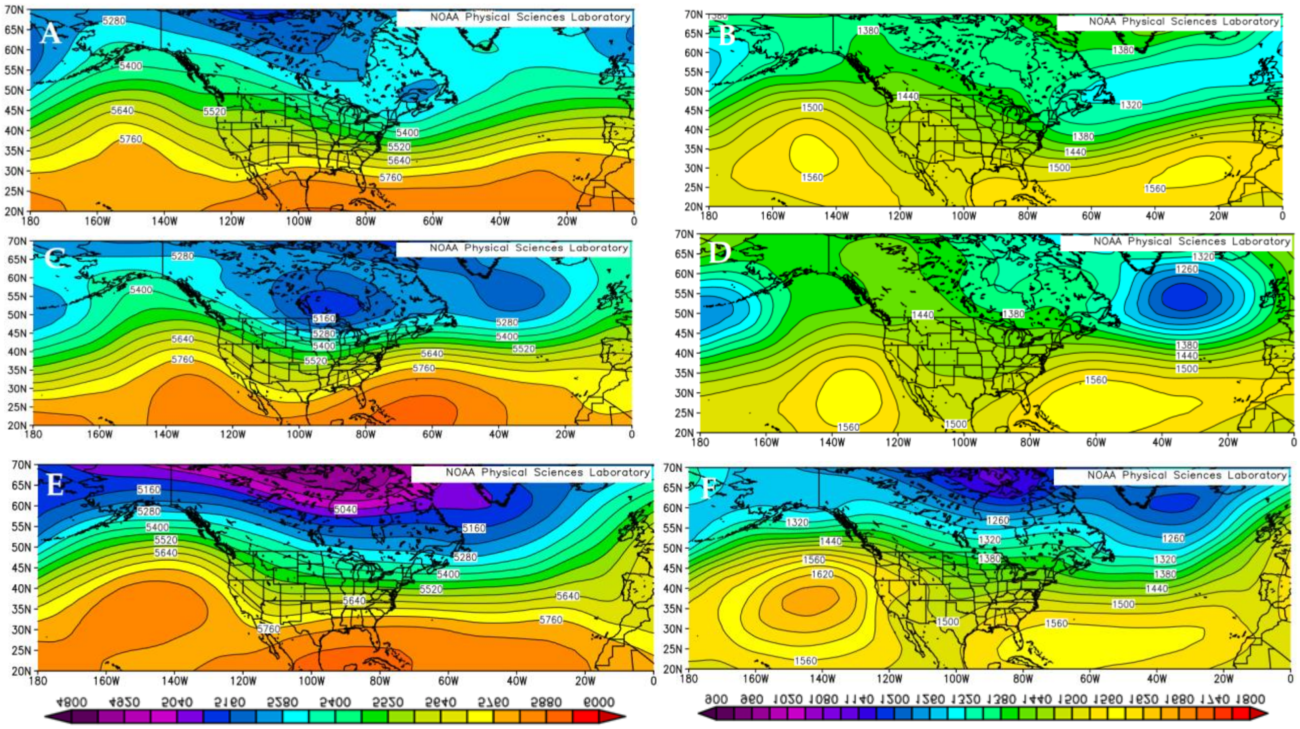

Figure 5. The 500 hPa height (m, **left**) and 850 hPa height (m, **right**) for 15 January to 28 February 2021 periods in Table 3. The contour intervals are 60 m and 30 m, respectively. Panels (**A,B**), (**C,D**), and (**E,F**) are for Periods 7–9, respectively.

Then, during Period 8, a deeper 500 hPa low pressure over southern Canada brought colder air into the central USA (Figure 5C) and this is evident at 850 hPa as well (Figure 5D). During this period, there was a blocking event in the northeast Pacific during the first part of this time-frame, while an Atlantic block over northwest Europe dominated the last part of the Period 8 (Table 2). The NH flow during this period was more meridional (see Figure 3c) than the time periods previous to and following it. Tables 4 and 5 demonstrate that this period was characterized by severe cold and snow, in spite of the generally drier conditions in the middle part of the USA. Even the southernmost stations received snow including more than half a meter in central Arkansas (LIT). However, the historic cold penetrated even farther to the south (Tables 4 and 5) reaching the Gulf Coast (EPA).

Period 8 can be sub-divided between the time before the onset of the Atlantic block and near the time of the 10 February IE Maximum. A distinct change in the NH flow took place after this maximum (Table 1 and Figure 3c) and the flow would move toward a more zonal state. Also, the time-period after the IE maximum represents a brief 5-day period of overlap between the lifecycle of the Pacific and Atlantic blocking events. Examining the temperature regime changes demonstrates (Tables 4 and 5) that the northern and western parts of the central USA became colder (1 °C to 4 °C), but the eastern and southern parts became dramatically colder (5 °C to 8 °C). In DFW and LIT, the temperature was about 10 °C or more colder during the second part of Period 8. Additionally, the second part of the cold wave was considerably wetter and snowier than the first part (Tables 4 and 5), except for southern Iowa.

After the NH flow regime showed a distinctive change in character following the IE maximum of 16 February (see Table 1 and Figure 3a,c), the flow over North America became more zonal in spite of a stronger Pacific Region ridge (Figure 5E,F). The trough over the central USA was no longer present. This period marked the return of anomalously warm weather over the region (Tables 4 and 5), but drier conditions than typical for the time of year, except for the two southernmost stations.

3.3. Discussion

The study of [18] highlighted weather for the region examined here during fixed 10-day periods of time before and after well-forecast IE maxima to demonstrate the ability of a forecast ensemble model to anticipate NH flow regime changes and their impact on local weather. Here, we examine flow regime and surface weather changes more closely during February and March 2019, highlighting the NH flow regime between IE maxima, and the changes before and after the IE maxima, any associated blocking events, as well as their connection to regional weather. Most of the IE maxima were well-forecast in [18].

The February and March 2019 time-frame was unique in recent years as both the East Pacific and Atlantic experienced a blocking episode that dominated over an approximate 7-week epoch from mid-February to early April 2019. Separately, the blocking episodes nearly dominate an entire season similar to the western Russia 2010 summer blocking episode (see [52] and references therein). In this instance, there were simultaneously occurring blocking events within each ocean basin during most of the time. After the 9 February 2019 IE maximum, the NH flow changes resulted in a local change of weather over the study region and even reaching down into the south-central USA.

In fact, as stated in Section 3.2, the first pair of simultaneously occurring blocking events in late February and early March were the 10th strongest to occur as measured by summing the BI quantity for each event since the mid-to-late 20th century (Period 3). This period was markedly colder, approximately one to two standard deviations below normal for late February and early March 2019 [4,51]. The onset of the blocking events occurred following the IE maximum of 18 February 2019, the Pacific region event occurring close to the time of the 25 February 2019 IE maximum. The Atlantic block came to an end in early March, while the Pacific region one decayed by 10 March 2019.

Following the end of these blocking events and the IE maximum of 7 March 2019, NH flow regime and the weather over the region warmed abruptly as noted in Section 3.2. Then, in mid-to-late March, two blocking events onset over the Atlantic and Pacific within 48 h of each other between 16 and 18 March 2019, and eastern North America was located under the trough between them (Period 5). What was remarkable about these two events was that the Pacific Region event occurred over western North America, and this time, only the eastern part of the region cooled substantially in association with the simultaneous blocking events. The two Period 5 blocking events were located in closer proximity than the first pair of blocking events during Period 3.

These simultaneous events came to an abrupt end at the same time (0000 25 March—Table 2) similar to the events studied in Lupo 1997. This study and others (e.g., [35,41]) have noted that blocking tends not to survive large-scale or NH flow regime transitions, although [43] found that long-lived blocking events can survive a flow transition as marked by an IE maximum as long as the blocking event was intensifying at the same time (e.g., [19] also). The Atlantic event weakens from around BI = 4 to BI = 2.8 and the Pacific event weakens marginally (from BI = 4.1 to BI = 3.5) except for the very last day (Figure 6A,B).

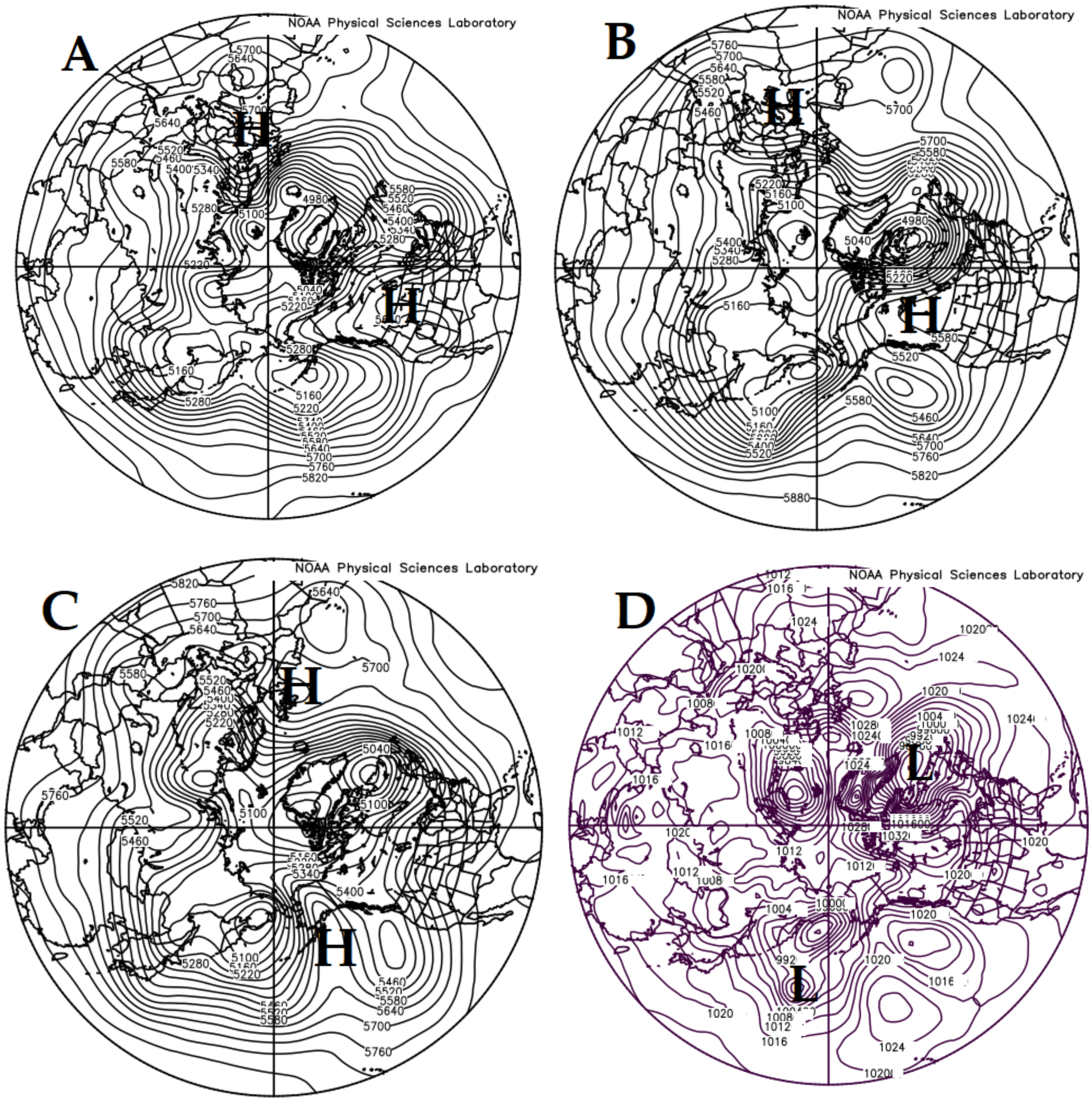

Figure 6. The 500 hPa height (m) maps for the NH at (**A**) 1200 UTC 22 March, (**B**) 1200 UTC 24 March, (**C**) 1200 UTC 26 March 2019, and (**D**) sea level pressure (hPa) for 1200 UTC 24 March 2019. The contour interval for height is 60 m and sea level pressure is 4 hPa. The H marks the center of blocking events, while in (**D**) L is the center of a surface low upstream of an incipient blocking.

Additionally, note in Table 2 and Figure 6 that the onset of successor blocking events (Period 6) occurred upstream (Figure 6C) of the onset location of these blocking event and certainly upstream of where the blocking events of 16–25 March were located at 1200 UTC 24 March (Figure 6B), in the Atlantic (15° E) and the Pacific (115° W), respectively. The successor events were distinct from the Period 5 events as determined using the criterion of [49] (and previous studies from this group). The synoptic-scale forcing associated with the onset of the successor blocking events and the accompanying upstream cyclones (Figure 6D) were located well upstream (more than 50° longitude) of the decaying events as suggested by [40], and the scenario resembles a block decay paradigm described in [38] where the large-scale flow regime changes were accompanied by a lack of synoptic scale support (See Figure 2, Figure 4, Figure 6, and Table 1).

Finally, the results of [18] imply that under some circumstances the decay of blocking can be anticipated relatively well. Since the IE maximum of 24 March was well forecast by the modelling system used in [18], knowing that blocking had persisted on 18 March, it is suggested that a forecaster could have anticipated the decay of the two events that were occurring about a week in advance. The work of [31] showed mixed results in anticipating decay, since blocking is routinely under-forecast in intensity and duration. The work of [33,52], and references such as [53] and [54] suggest it is difficult to forecast block decay in the long-term. Here, it is suggested (in concert with [18]) that block decay can be anticipated within a 7-day period, especially in conjunction with the event weakening.

The case of February 2021 was unusual in that much of the winter was from 1 December to 28 February was warmer than the seasonal normal for all but mid-February 2021. Mid-February 2021 was a historic cold period in both depth and length. For example, at the Columbia, MO station, the temperature stayed below 0 °C for 14 straight days and below −7 °C for 11 straight days. The former was the 12th longest such period on record for this station, while the latter was tied for the longest such period, respectively since 1889 [55]. Such a severe cold wave has not been noted over the region since at least the 1980s and other cities (e.g., Wichita, Kansas—ICT) experienced similarly long periods of cold [6]. This was associated with costly impacts on the US economy [7].

During the cold outbreak event, the Pacific Region blocking was identifiable in the upper troposphere above 500 hPa (Figure 7C,D). Blocking events have been observed to impact the flow into the lower stratosphere [14–17]. Additionally, blocking can influence the amount of trace gases in the upper troposphere and lower stratosphere which are a reflection of tropospheric dynamics, but also influences the temperature structure aloft [56,57]. During Period 7, the strong polar low pressure area at 100 hPa is located firmly in the eastern NH (Figure 7A,B) and positive height anomalies (Figure 7B) are located over Greenland with a weaker one over the Gulf of Alaska. Both are roughly coincident with shorter-lived blocking events that occurred during this time (Table 2) and the stronger Atlantic block is associated with the stronger anomaly.

Then during the 3–15 February blocking, strong positive 100 hPa height anomalies were found in the Gulf of Alaska region and poleward (Figure 7C,D), while a negative height anomaly was located over the southern Canada and the northern USA. The Pacific Region blocking event can be classified as strong using the BI (see [49]). The weaker Atlantic blocking which was associated with the latter part of the cold wave cannot be identified at 100 hPa and a more widespread negative height anomaly is located over NA (Figure 7E,F). By the latter part of the cold outbreak, the core of the polar low pressure is located over the western part of the NH.

Finally, the work of [26] demonstrated that over Eurasia, different large-scale NH flow regimes could be associated with particular seasons. Such transitions were identifiable in the NH flow between spring and summer as represented by examining time series of IE [23] or large-scale wave amplitude energy [24]. These studies involved about 10 NH spring and summer seasons. If the IE record used for [18] is examined (May 2018–April 2019), there is a distinct annual cycle in the IE (not shown) and the mean July and August 2018 NH IE values were more than one standard deviation below the annual average. The February 2019 values were more than one standard deviation above the annual mean with January and March 2019 being about one-half standard deviations above the annual mean (see Section 3.1.1 above). If the spring-to-summer transition criterion of [23] were applied to 2018, a transition in early June can be identified in the NH IE. A similar transition between the winter (February 2019) and early part of the spring (March 2019) may be present in the NH IE time series studied here, as the mean for March is clearly lower than February. This suggests the possibility of a winter–spring transition (as in [26]), especially in light of the large change in sensible weather over the central USA in early March. However, more seasons would need to be studied in order to confirm this conjecture.

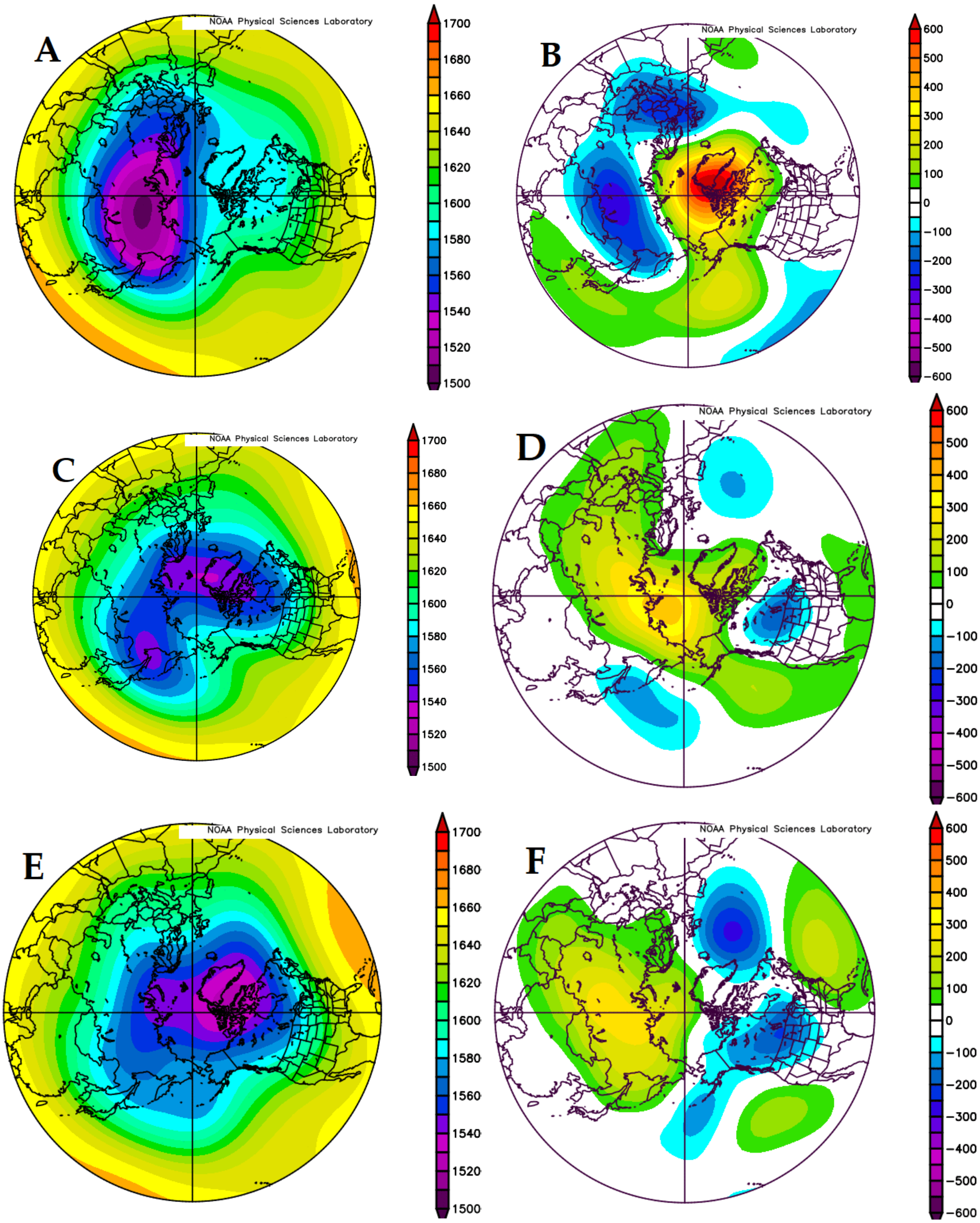

Figure 7. The 100 hPa (**A**,**C**,**E**) height (dam) and (**B**,**D**,**F**) height anomalies (m) for (**A**,**B**) 17–29 January 2021 (Period 7), (**C**,**D**) 3–15 February 2021 (Pacific Region block), and (**E**,**F**) 11–21 February 2021 (Atlantic Region block). The contour interval in the height figures is 10 dam and anomaly figures is 50 m.

4. Conclusions

In this study, two late winter cold air outbreaks over the central USA were studied in order to identify their occurrence in association with blocking onset and termination, changes in teleconnection character, and the occurrence of IE maxima in the NH flow. This study used the NCEP re-analyses, teleconnection time series, and an archive of blocking events located at the University of Missouri. The February and March 2019 cold air outbreak was associated with simultaneous blocking episodes over the Atlantic and Pacific regions persisting from early February to early April. The deep cold air outbreak of February 2021 was also examined. This event occurred inside a winter season that was relatively mild otherwise.

The analysis of the large-scale flow demonstrated that for the 2019 and 2021 cases, that IE maxima could be used to identify changes in the NH flow as shown in past studies. The IE maxima were often, but not always, associated with the onset and termination of blocking events which has also been demonstrated previously. Also, we associated the IE maxima with changes in the tendencies of three primary teleconnection indexes (AO, NAO, and PNA) that influence North American weather. The slope of the index time series either decreased or increased strongly or changed sign concurrent with the occurrence of an IE maximum.

However, we have associated these large-scale flow regimes with distinct regimes of surface weather (temperature and precipitation) occurring in the central USA. In particular, the strength of a surface cold air outbreak seems to be associated with the strength of the upstream Pacific region blocking or upstream blocking in association with Atlantic Region blocking (simultaneous blocking). The coldest air during the 2019 period was associated with the 10th strongest simultaneous blocking pair in the 54-year blocking archive used in this study. Other periods of blocking were associated with weaker cooling.

In 2021, the second half of the cold outbreak was clearly associated with larger cold air anomalies, and this followed a 5-day overlap between the associated Pacific region blocking event occurring mainly during the early part of the cold outbreak and an Atlantic event which occurred mainly during the second half of the outbreak.

During the 2019 and 2021 cold air event, the core of the cold air outbreak reached into the southern plains as qualitatively determined using a weather station in northeast Texas. The 2021 event was particularly severe. The 2021 event was associated with a deep Pacific Region blocking event that was present in the upper troposphere and lower stratosphere. This blocking event likely aided the migration of the 100 hPa polar low pressure from the eastern NH to the western NH.

An examination of the decay of a pair of simultaneously occurring blocking events which terminated together within 24 h of a NH IE maximum demonstrated that the inability of most blocking events to survive NH large-scale flow transitions make blocking decay somewhat predictable. This conclusion is reached using the results of the current study and the study of [18] which showed that IE maxima were well-forecast 7 days in advance generally in an ensemble forecasting system. At the time, both blocking events were generally weakening. Both events were succeeded by a blocking event which developed upstream of the onset location of the two events which decayed.

Lastly, there was a detectable change in the magnitude of the NH IE time series from February 2019 and March 2019 that would indicate the possibility of a winter-to-spring transition similar to identified spring-to-summer transition of seasons documented by earlier published studies. In both of the cases studied here, the regional weather following both late-winter cold air outbreaks returned to conditions that were considered normal for the time of the season, and similar to the character of the pre-cold outbreak weather type. More seasons should be studied in order to determine whether a winter-to-spring transition in the magnitude of the IE time series (or wave amplitude index) can be identified similar to the spring-to-summer, as shown in earlier studies.

Author Contributions: Conceptualization, M.A.E., S.M. and A.R.L.; methodology, A.R.L.; software, M.A.E., S.M., C.A.S. and A.R.L., validation, M.A.E., S.M. and A.R.L.; formal analysis, M.A.E., S.M., C.A.S. and A.R.L.; investigation, M.A.E., S.M., C.A.S. and A.R.L.; resources, A.R.L.; data curation, A.R.L.; writing—original draft preparation, M.A.E., S.M. and A.R.L.; writing—review and editing, M.A.E., S.M., C.A.S. and A.R.L.; visualization, M.A.E., S.M., C.A.S. and A.R.L.; supervision, A.R.L.; project administration, A.R.L. All authors have read and agreed to the published version of the manuscript.

Funding: This research received no external funding.

Institutional Review Board Statement: Not applicable.

Informed Consent Statement: Not applicable.

Data Availability Statement: The data used for the surface weather is available via the National Weather Service (http://weather.gov accessed on 15 February 2022). The IE and teleconnection calculations, as well as the blocking data, and the data for each period in Section 3.2 are archived on a computer in the Global Climate Change Laboratory and the Weather Analysis and Visualization Laboratory at the University of Missouri (http://weather.missouri.edu accessed on 15 February 2022).

Acknowledgments: The authors would like to thank the two anonymous reviewers for their time and effort in making this a stronger contribution.

Conflicts of Interest: The authors declare no conflict of interest.

References

1. Quiroz, R.S. The climate of the 1983-84 winter. A season of strong blocking and severe cold in North America. *Mon.Weather Rev.* **1984**, *112*, 1894–1912. [CrossRef]
2. Whan, K.; Zwiers, F.; Sillmann, J. The Influence of Atmospheric Blocking on Extreme Winter Minimum Temperatures in North America. *J. Clim.* **2016**, *29*, 4361–4381. [CrossRef]
3. Nunes, M.J.; Lupo, A.R.; Lebedeva, M.; Chendev, Y.G.; Solovyov, A.B. The Occurrence of Extreme Monthly Temperatures and Precipitation in Two Global Regions. *Pap. Appl. Geogr.* **2017**, *3*, 143–156. [CrossRef]
4. Renken, J.; Herman, J.J.; Bradshaw, T.R.; Market, P.S.; Lupo, A.R. The Utility of the Bering Sea and East Asia Rules in Long-Range Forecasting. *Adv. Meteorol.* **2017**, *2017*, 1–14. [CrossRef]
5. National Climatic Data Center. Available online: https://www.ncdc.noaa.gov/temp-and-precip/us-maps/1/202102#us-maps-select (accessed on 3 December 2021).
6. National Weather Service specifically for 2021 case office at Wichita, KS. Available online: https://www.weather.gov/ict/historicCold (accessed on 3 December 2021).
7. The Perryman Group. Available online: https://www.perrymangroup.com/media/uploads/brief/perryman-preliminary-estimates-of-economic-costs-of-the-february-2021-texas-winter-storm-02-25-21.pdf (accessed on 3 December 2021).
8. Yao, Y.; Luo, D.; Dai, A.; Simmonds, I. Increased quasi stationarity and persistence of Ural blocking and Eurasian extreme cold events in response to Arctic warming. Part I: Insight from observational analyses. *J. Clim.* **2017**, *30*, 3549–3568. [CrossRef]
9. Luo, D.; Xiao, Y.; Yao, Y.; Dai, A.; Simmonds, I.; Franzke, C.L. Impact of Ural blocking on winter warm Arctic–cold Eurasian anomalies. Part I: Blocking-induced amplification. *J. Clim.* **2016**, *29*, 3925–3947. [CrossRef]
10. Sousa, P.M.; Trigo, R.; Barriopedro, D.; Soares, P.; dos Santos, J.C.A. European temperature responses to blocking and ridge regional patterns. *Clim. Dyn.* **2017**, *50*, 457–477. [CrossRef]
11. Sillmann, J.; Croci-Maspoli, M.; Kallache, M.; Katz, R.W. Extreme cold winter temperatures in Europe under the influence of North Atlantic atmospheric blocking. *J. Clim.* **2011**, *24*, 5899–5913. [CrossRef]
12. Ratnam, J.V.; Behera, S.K.; Annamalai, H.; Ratna, S.B.; Rajeevan, M.; Yamagata, T. ENSO's far reaching connection to Indian cold waves. *Nat. Sci. Rep.* **2016**, *6*, 37657. [CrossRef]
13. Efe, B.; Lupo, A.R.; Deniz, A. Extreme Temperatures linked to the Atmospheric Blocking Events in Turkey between 1977–2016. *Nat. Hazards* **2019**, *104*, 1879–1898. [CrossRef]
14. Quiroz, R.S. The association of stratospheric warmings with tropospheric blocking. *J. Geophys. Res.* **1986**, *91*, 5277–5285. [CrossRef]
15. Martius, O.; Polvani, L.M.; Davies, H.C. Blocking precursors to stratospheric sudden warming events. *Geophys. Res. Lett.* **2009**, *36*, 14. [CrossRef]
16. Colucci, S.J.; Kelleher, M.E. Diagnostic comparison of tropospheric blocking events with and without sudden stratospheric warming. *J. Atmos. Sci.* **2015**, *72*, 2227–2240. [CrossRef]
17. Attard, H.E.; Lang, A.L. Troposphere–Stratosphere Coupling Following Tropospheric Blocking and Extratropical Cyclones. *Mon. Wea. Rev.* **2019**, *147*, 1781–1804. [CrossRef]
18. Klaus, E.M.; Market, P.S.; Lupo, A.R.; Bodner, M.J.; Kastman, J.S. Projecting Northern Hemisphere Flow Regime Transition Using Integrated Enstrophy. *Atmosphere* **2020**, *11*, 915. [CrossRef]

19. Jensen, A.D.; Lupo, A.R.; Mokhov, I.I.; Akperov, M.G.; Reynolds, D.D. Integrated regional enstrophy and block intensity as a measure of Kolmogorov Entropy. *Atmosphere* **2017**, *8*, 237. [CrossRef]
20. Jensen, A.D.; Lupo, A.R.; Mokhov, I.I.; Akperov, M.G.; Sun, F. The dynamic character of Northern Hemisphere flow regimes in a near term climate change projection. *Atmosphere* **2018**, *9*, 27. [CrossRef]
21. European Centre for Medium-Range Weather Forecast. *Annual Report 2017. European Centre for Medium-Range Weather Forecast*; European Centre for Medium-Range Weather Forecast: Reading, UK, 2018; pp. 1–40.
22. Krishnamurthy, V. Predictability of Weather and Climate. *Earth Space Sci.* **2019**, *6*, 1043–1056. [CrossRef]
23. Newberry, R.G.; Lupo, A.R.; Jensen, A.D.; Rodgriges–Zalipynis, R.A. An analysis of the spring-to-summer transition in the West Central Plains for application to long range forecasting. *Weather Clim. Sci.* **2016**, *6*, 373–393. [CrossRef]
24. Hansen, A.R. Observational Characteristics of Atmospheric Planetary Waves with Bimodal Amplitude Distributions. *Adv. Geophys.* **1986**, *29*, 101–134.
25. Ratley, C.W.; Lupo, A.R.; Baxter, M.A. Determining the spring to summer transition in the Missouri Ozarks using synoptic scale atmospheric data. *Trans. Mo. Acad. Sci.* **2002**, *36*, 69–76.
26. Kononova, N.K.; Lupo, A.R. Investigation of the variability of circulation regimes and dangerous weather phenomena in Russia in the 21st century. IOP Science Conf Ser. *Earth Environ. Sci.* **2020**, *606*, 012023.
27. Konrad, C.E.; Colucci, S.J. Synoptic climatology of 500-mb circulation changes during explosive cyclogenesis. *Mon. Weather Rev.* **1988**, *116*, 1431–1443. [CrossRef]
28. Tsou, C.H.; Smith, P.J. The role of synoptic/planetary-scale interactions during the development of a blocking anticyclone. *Tellus* **1990**, *42A*, 174–193. [CrossRef]
29. Tracton, M.S. Predictability and its relationship to scale interaction processes in blocking. *Mon. Weather Rev.* **1990**, *118*, 1666–1695. [CrossRef]
30. Tibaldi, S.; Molteni, F. On the operational predictability of blocking. *Tellus* **1990**, *42*, 343–365. [CrossRef]
31. Reynolds, D.D.; Lupo, A.R.; Jensen, A.D.; Market, P.S. The predictability of Northern Hemispheric blocking using an ensemble mean forecast system. *Open Atmos. Sci. J.* **2019**, *13*, 3–17. [CrossRef]
32. Woollings, T.; Barriopedro Cepero, D.; Methven, J.; Son, S.-W.; Martius, O.; Harvey, B.; Sillmann, J.; Lupo, A.R.; Seneviratne, S. Blocking and its response to climate change. *Curr. Clim. Chang. Rep.* **2018**. [CrossRef]
33. Lupo, A.R. Atmospheric Blocking Events: A Review. *Ann. N. Y. Acad. Sci.* **2021**, *1504*, 5–24. [CrossRef]
34. Hoskins, B. A potential vorticity view of synoptic development. *Meteorol. Appl.* **1997**, *4*, 325–334. [CrossRef]
35. Haines, K.; Holland, A.J. Vacillation cycles and blocking in a channel. *Q. J. R. Meteorol. Soc.* **1998**, *124*, 873–897. [CrossRef]
36. Colucci, S.J.; Baumhefner, D.P. Numerical prediction of the onset of blocking: A case study with forecast ensembles. *Mon. Weather Rev.* **1998**, *126*, 773–784. [CrossRef]
37. Luo, D. Planetary-scale baroclinic envelope Rossby solitons in a two-layer model and their interaction with synoptic-scale eddies. *Dyn. Atmos. Ocean.* **2000**, *32*, 27–74. [CrossRef]
38. Lupo, A.R.; Mokhov, I.I.; Dostoglou, S.; Kunz, A.R.; Burkhardt, J.P. The impact of the planetary scale on the decay of blocking and the use of phase diagrams and enstrophy as a diagnostic. *Izv. Atms -Oc.* **2007**, *43*, 45–51. [CrossRef]
39. Hussain, A.; Lupo, A.R. Scale and stability analysis of blocking events from 2002–2004: A case study of an unusually persistent blocking event leading to a heat wave in the Gulf of Alaska during August 2004. *Adv. Meteorol.* **2010**, *2010*, 610263.
40. Lupo, A.R.; Bosart, L.F. An analysis of a relatively rare case of continental blocking. *Q. J. R. Meteorol. Soc.* **1999**, *125*, 107–138. [CrossRef]
41. Lupo, A.R. A diagnosis of two blocking events that occurred simultaneously over the mid-latitude Northern Hemisphere. *Mon. Weather Rev.* **1997**, *125*, 1801–1823. [CrossRef]
42. Burkhardt, J.P.; Lupo, A.R. The planetary and synoptic-scale interactions in a Southeast Pacific blocking episode using PV diagnostics. *J. Atmos. Sci.* **2005**, *62*, 1901–1916. [CrossRef]
43. Jensen, A.D. The non-equilibrium thermodynamics of blocking. *Atmos. Chem. Phys. Discuss.* **2016**. [CrossRef]
44. NCEP/NCAR Reanalyses Project. Available online: http://www.esrl.noaa.gov/psd/data/reanalysis/reanalysis.shtml (accessed on 6 May 2019).
45. University of Missouri Blocking Archive. 2021. Available online: http://weather.missouri.edu/gcc/ (accessed on 3 December 2021).
46. Climate Diagnostic Bulletin. Available online: https://www.cpc.ncep.noaa.gov/products/CDB/CDB_Archive._pdf/pdf_CDB_archive.shtml (accessed on 13 May 2019).
47. Climate Prediction Center: Weather and Climate Linkages. Available online: https://www.cpc.ncep.noaa.gov/products/precip/CWlink/daily_ao_index/teleconnections.shtml (accessed on 12 May 2020).
48. Balkissoon, S.S.; Bongard, J.T.; Cain, T.; Candela, D.M.; Clay, C.; Efe, B.; Ji, Q.; Klaus, E.M.; Korner, A.P.; Mitchell, K.; et al. 2020: Hurricane Florence Makes Landfall in the Southeast USA: Sensitive Dependence on Initial Conditions, Parameterizations, and Integrated Enstrophy. *Atmos. Clim. Sci.* **2020**, *10*, 101–124.
49. Lupo, A.R.; Jensen, A.D.; Mokhov, I.I.; Timazhev, A.V.; Eichler, T.; Efe, B. Changes in global blocking character during the most recent decades. *Atmosphere* **2019**, *10*, 92. [CrossRef]
50. Lupo, A.R.; Kononova, N.K.; Semenova, I.G.; Lebedeva, M.G. A comparison of the characteristics of drought during the late 20th and early 21st centuries over Eastern Europe, Western Russia and Central North America. *Atmosphere* **2021**, *12*, 33. [CrossRef]

51. Lupo, A.R.; Kelsey, E.P.; McCoy, E.A.; Halcomb, C.E.; Aldrich, E.; Allen, S.N.; Akyuz, A.; Skellenger, S.; Beiger, D.G.; Wise, E.; et al. The presentation of temperature information in television broadcasts: What is normal? *Natl. Weather Dig.* **2003**, *27*, 53–58.
52. Lupo, A.R.; Mokhov, I.I.; Akperov, A.G.; Chernokulsky, A.V.; Hussain, A. A dynamic analysis of the role of the planetary and synoptic scale in the summer of 2010 blocking episodes over the European part of Russia. *Adv. Meteorol.* **2012**, *2012*, 584257. [CrossRef]
53. Matsueda, M. Blocking predictability in operational medium-range ensemble forecasts. *SOLA* **2009**, *5*, 113–116. [CrossRef]
54. Matsueda, M. Predictability of Euro-Russian blocking in summer of 2010. *Geophys. Res. Lett.* **2011**, *38*. [CrossRef]
55. Missouri Climate Center. 2021. Available online: http://climate.missouri.edu/ (accessed on 12 May 2021).
56. Sitnov, S.A.; Mokhov, I.I.; Lupo, A.R. Evolution of the water vapor plume over Eastern Europe during summer 2010 atmospheric blocking. *Adv. Meteorol.* **2014**, *2014*, 253953. [CrossRef]
57. Sitnov, S.; Mokhov, I.I.; Lupo, A.R. Ozone and water vapor anomalies during atmospheric blocking events over European Russia in Spring and Summer 2010. *Atmos. Environ.* **2017**, *164*, 180–194. [CrossRef]